LETTER TO THE EDITOR

Spatial relationship of tertiary lymphoid structures and tumor-associated neutrophils in bladder cancer and prognostic potential for anti-PD-L1 immunotherapy

Dear Editor,

Tertiary lymphoid structures (TLSs) are organized clusters of immune cells found in non-lymphoid tissues of chronic inflammation, including solid tumors [1]. High endothelial venules (HEVs) positive for peripheral node addressin (PNAd) are present in TLSs and may provide highway entry for lymphocytes. Tumor-residing TLSs may be formed by the concerted actions of cytokines and chemokines, a finding supported by the relation between a 12-chemokine signature and TLSs [2]. C-X-C motif chemokine ligand 13 (CXCL13) is central in TLS formation in tumors, including bladder cancer [3]. TLSs are associated with favorable prognoses in cancer and favorable responses to immune checkpoint blockade (ICB) independent of programmed death-ligand 1 (PD-L1) status [4]. TLSs may also contain immunosuppressive cells such as regulatory T cells and regulatory B cells. A prominent immunosuppressive population is polymorphonuclear myeloid-derived suppressor cells (PMN-MDSCs), which are essentially tumor-associated neutrophils (TANs) that suppress effector T cells [5]. The relative distribution of TLSs and TANs/PMN-MDSCs has not been studied in human cancers.

We designed a study to investigate the distribution of immune cells (especially TANs/PMN-MDSCs) inside and near the TLSs of bladder cancer (the 10th most common cancer worldwide) and to evaluate the prognostic signifi-

cance of TLSs and TANs/PMN-MDSCs in bladder cancer patients treated with ICB therapy. We performed a retrospective study using formalin-fixed paraffin-embedded samples from 26 primary bladder cancers (Supplementary Table S1, Supplementary Methods). Samples were stained with hematoxylin-and-eosin (H&E) to recognize 58 TLS regions of interest (ROIs), which were further stained with 14 cell markers with MultiOmyx (Figure 1A, Supplementary Table S2). The co-staining patterns allowed the identification of various immune populations, including TANs (Supplementary Figure S1A, Supplementary Table S3). The 58 TLSs were classified into 23 early TLSs (E-TLSs) and 35 follicle-like TLSs (FL-TLSs) based on the morphology: E-TLSs contained less organized B cells and T cells in an irregularly shaped region and very few (or no) PNAd$^+$ HEVs, whereas FL-TLSs had demarcated a B-cell zone and a T-cell zone in a follicular structure interspersed with several HEVs (Figure 1B). As expected, FL-TLSs contained higher densities of B cells and extended larger areas than E-TLSs (Figure 1C).

To examine the spatial distribution and interrelationship of immune cells relative to TLSs, we set the TLS-ROIs as the center and selected ROIs 500 μm and 1,000 μm away as near-TLS-ROIs and far-TLS-ROIs (Figure 1D). We compared the immune cell densities in the three ROI types (Figure 1E). Lymphocytes, including B, CD4$^+$ T, CD8$^+$ T and regulatory T (Treg), were most abundant in the TLS-ROIs and decreased as the distance from TLSs increased. Similar patterns were observed for human leukocyte antigen (HLA)-DR$^-$ [major histocompatibility complex (MHC)-II$^-$] myeloid cells, C-X-C chemokine receptor 2 (CXCR2)$^+$MHC-II$^-$ myeloid cells, and TANs (Figure 1E). CXCR2 is a predominant chemokine receptor for PMN-MDSCs in bladder cancer [6]. About 10%-30% of TANs were CXCR2$^+$ (Supplementary Figure S1B). For FL-TLSs, the densities of lymphocytes, MHC-II$^-$ myeloid cells and TANs followed the TLS>near>far pattern (Figure 1F). For E-TLSs, lymphocyte densities remained highest in
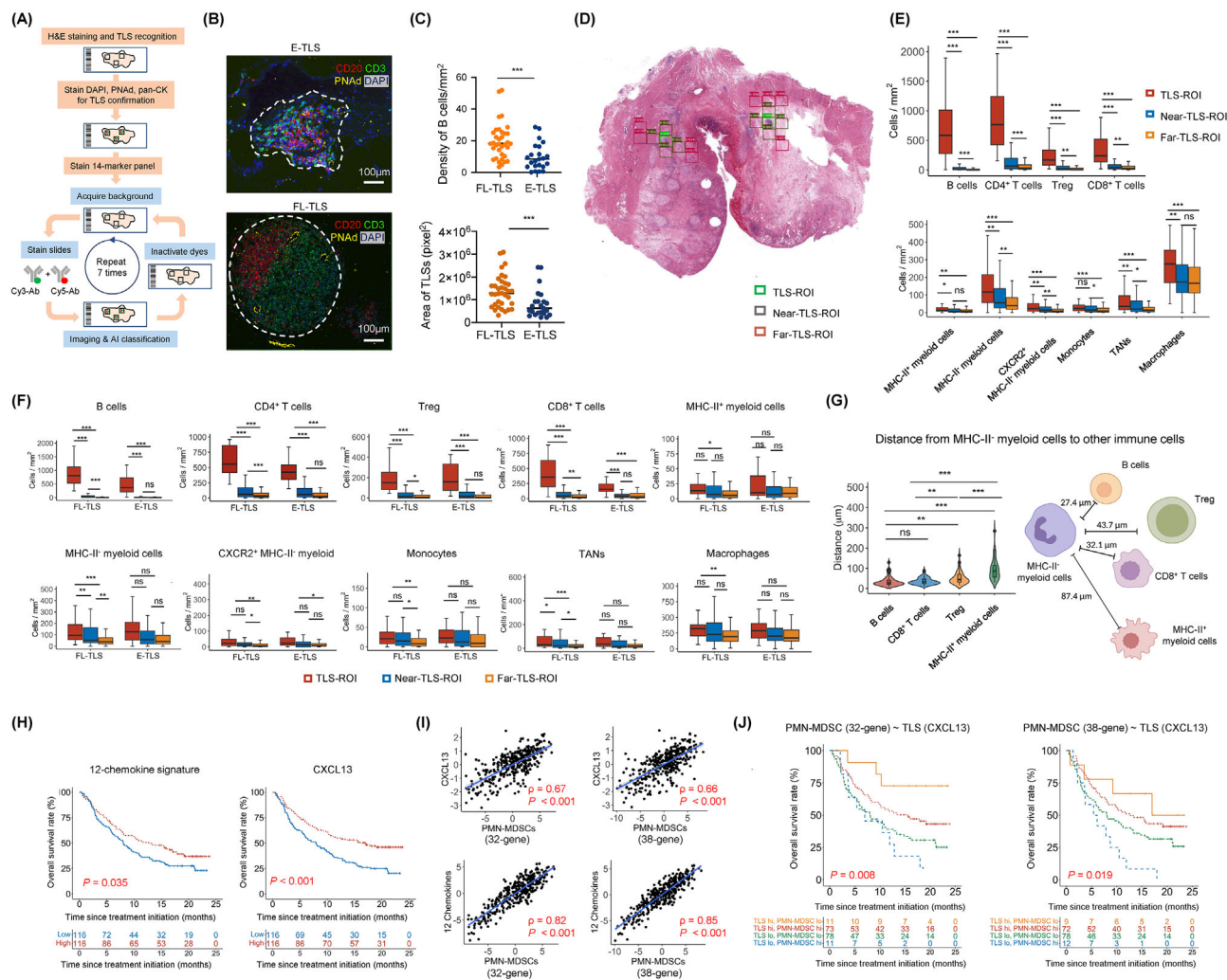
FIGURE 1 MultiOmyx and *in silico* analysis of TLSs and immune populations in bladder cancer. (A) Project workflow with MultiOmyx. (B) Representative MultiOmyx images of E-TLS and FL-TLS. TLS region was contoured with white dash lines. (C) Densities of B cells in E-TLS and FL-TLS in TLS-containing ROIs (upper). TLS area sizes of E-TLS and FL-TLS in TLS-ROIs (lower). *P* values were calculated with Mann Whitney U test. (D) Representative H&E section marked with two TLS-ROIs (green) surrounded by multiple near-TLS-ROIs (purple) and far-TLS-ROIs (pink). (E) Comparison of the densities of various lymphocyte and myeloid populations in TLS-ROIs, near-TLS-ROIs and far-TLS-ROIs. *P* values were calculated with Kolmogorov-Smirnov test. The box limits are the lower and upper quantiles, and the whiskers extend to the most extreme values within 1.5 x IQR. (F) More refined comparison of the densities of lymphocyte and myeloid populations based on both ROI types (TLS, near, far) and TLS stages (E-TLS, FL-TLS). The box limits are the lower and upper quantiles, and the whiskers extend to the most extreme values within 1.5 x IQR. (G) Violin plots showing the distances of MHC-II⁻ myeloid cells to B cells, CD8⁺ T cells, Treg and MHC-II⁺ myeloid cells in the TLS-ROIs, with the schematic illustrating the median distances. *P* values were calculated with Kolmogorov-Smirnov test. (H) Overall survival of the upper and lower tertiles of patients in IMvigor210 based on 12-chemokine genes signatures or CXCL13 expression. Log-rank test *P* values are marked. (I) Correlation of CXCL13 gene expression or 12-chemokine gene signature expression with either of the two PMN-MDSC gene signatures based on the IMvigor210 dataset. Spearman correlation coefficient *ρ* and *P* values are marked. (J) Kaplan-Meier analysis for overall survival of patients in IMvigor210 classified into four groups based on CXCL13 expression (TLS marker) and either of the two PMN-MDSC gene signatures. Upper and lower tertiles were classified as high (hi) and low (lo) for the signatures, respectively. *P* values based on two-sided log-rank tests are marked. In all the tests, * *P* < 0.05, ** *P* < 0.01, *** *P* < 0.001; ns, *P* > 0.05. AI, artificial intelligence, C-X-C chemokine receptor 2; CXCL13, C-X-C motif chemokine ligand 13; DAPI, 4′,6-diamidino-2-phenylindole; E-TLS, early tertiary lymphoid structure; FL-TLS, follicle-like tertiary lymphoid structure; H&E, hematoxylin-and-eosin; HLA-DR, human leukocyte antigen DR CXCR2, IQR, interquartile range; MHC-II, major histocompatibility complex class II; ns, not significant; PMN-MDSC, polymorphonuclear myeloid-derived suppressor cell; PNAd, peripheral node addressin; pan-CK, pan-cytokeratin; ROI, regions of interest; Treg, regulatory T; TAN, tumor-associated neutrophil; TLS, tertiary lymphoid structure.

TLS-ROIs, but showed no significant difference between near and far ROIs; the stepwise decreasing trend was present in myeloid cells but did not reach statistical significance (Figure 1F). Regarding cell-cell distances, MHC-II$^-$ myeloid cells were closest to B cells and CD8$^+$ T cells, followed by Treg, and farthest from MHC-II$^+$ myeloid cells (Figure 1G, Supplementary Table S4). Distances between MHC-II$^-$ myeloid cells and other immunocytes were shorter in TLS-ROIs than in near- or far-TLS-ROIs (Supplementary Figure S1C).

Given the density enrichment of TANs in TLSs and that many TANs function as PMN-MDSCs, we assessed the clinical association between TLSs and PMN-MDSCs using gene signatures based on the IMvigor210 phase 2 trial of atezolizumab (anti-PD-L1) on advanced urothelial carcinoma [7]. TLS signatures (12-chemokine [2] or CXCL13 [3]) were associated with better survival (Figure 1H, Supplementary Table S5). Both TLS signatures were positively correlated with a 32-gene PMN-MDSC signature [8] or a 38-gene PMN-MDSC signature [9] (Figure 1I, Supplementary Table S5). When patients were stratified based on both TLS and PMN-MDSC signatures, the survival from favorable to unfavorable followed the order TLS^{high}PMN-MDSC^{low} > TLS^{high}PMN-MDSC^{high} > TLS^{low}PMN-MDSC^{low} > TLS^{low}PMN-MDSC^{high} (Figure 1J). Note that the TLS^{high}PMN-MDSC^{low} and TLS^{low}PMN-MDSC^{high} groups had lower numbers of patients because the two signatures had opposite trends.

We tested the association of TLS signatures with two TAN signatures (Supplementary Table S5) in IMvigor210. Consistent with the PMN-MDSC signatures, both TAN signatures were positively correlated with TLS signatures (Supplementary Figure S1D), and overall survival followed the order TLS^{high}TAN^{low} > TLS^{high}TAN^{high} > TLS^{low}TAN^{low} > TLS^{low}TAN^{high} from favorable to unfavorable outcomes (Supplementary Figure S1E). We also tested the prognostic significance of TLS signatures alone or in conjunction with the PMN-MDSC signature in non-small cell lung cancer (NSCLC) treated with anti-PD-1/PD-L1 therapy [10]. TLS signatures were again associated with better overall survival (Supplementary Figure S1F) and with PMN-MDSC signature (Supplementary Figure S1G). When both signatures were used to stratify NSCLC patients, overall survival also followed the order TLS^{high}PMN-MDSC^{low} > TLS^{high}PMN-MDSC^{high} > TLS^{low}PMN-MDSC^{low} > TLS^{low}PMN-MDSC^{high} from favorable to unfavorable outcomes (Supplementary Figure S1H). Therefore, the TLS/PMN-MDSC prognostic association is also valid in anti-PD-1/PD-L1 antibody-treated NSCLC.

We stratified patients in IMvigor210 into basal and luminal subtypes based on a 47-gene signature (Supplementary Figure S2A, Supplementary Table S5). The luminal subset survived better than the basal subset (Supplementary Figure S2B). TLS^{high} patients in both subtypes survived better than TLS^{low} patients (Supplementary Figure S2C), and TLS signatures were correlated with PMN-MDSC signatures in both subtypes (Supplementary Figure S2D). TLS and PMN-MDSC levels assessed by signature expressions were higher in the basal than in the luminal subtype (Supplementary Figure S2E). TLS^{high}PMN-MDSC^{low} patients showed more favorable outcome than TLS^{low}PMN-MDSC^{high} patients in the basal subtype (Supplementary Figure S2F). The luminal subtype was difficult to assess in the same manner due to very few PMN-MDSC^{high} cases. Lastly, both TLS and PMN-MDSC signatures were associated with PD-1 or PD-L1 levels (Supplementary Figure S2G) and T cell pathways (PD-1- or exhaustion-related) in IMvigor210 (Supplementary Figure S2H).

Our study made two main discoveries. First, lymphocytes and immunosuppressive myeloid cells (especially TANs) were most abundant in mature TLSs of bladder cancer, with densities decreasing as the distance from TLSs increased. While we speculated that TAN density follows this gradient if TANs enter TLSs through HEVs and diffuse radially, an alternative model where TANs extravasating into the tumor bed enrich through a chemokine gradient toward TLSs may lead to the same result. Future experiments with cell tracing may answer which mechanism prevails. Second, patients with bladder cancer characterized as TLS^{high}PMN-MDSC^{low} and TLS^{low}PMN-MDSC^{high} showed the best and worst prognosis with anti-PD-L1 therapy, respectively. These results may have the following clinical implications: (i) an immune score based on TLS^{high}PMN-MDSC^{low} may help select patients who would benefit most from ICB therapy; (ii) for TLS^{low}PMN-MDSC^{high} patients, strategies to induce TLS formation and debilitate PMN-MDCSs may help overcome ICB therapy resistance.

DECLARATIONS

AUTHOR CONTRIBUTIONS

Xuechun Wang, Anna Juncker-Jensen: Conceptualization, investigation, methodology, data curation, formal analysis, validation, visualization, writing – original draft, writing – review & editing.

Gang Huang, Mate Levente Nagy: Investigation, formal analysis.

Xuemin Lu: Formal analysis, supervision.

Liang Cheng, Xin Lu: Conceptualization, resources, supervision, funding acquisition, project administration, writing – original draft, writing – review & editing.

ETHICS APPROVAL AND CONSENT TO PARTICIPATE

The experiments were approved by the Institutional Review Board of Indiana University School of Medicine and University of Notre Dame (#1808872882).

CONSENT FOR PUBLICATION

Not applicable.

DATA AVAILABILITY STATEMENT

The data presented in this study are available for request from the corresponding authors.

Xuechun Wang[1]
Anna Juncker-Jensen[2]
Gang Huang[1]
Mate Levente Nagy[2]
Xuemin Lu[1]
Liang Cheng[3]
Xin Lu[1,4]

[1]*Department of Biological Sciences, Boler-Parseghian Center for Rare and Neglected Diseases, Harper Cancer Research Institute, University of Notre Dame, Notre Dame, IN, USA*
[2]*NeoGenomics Laboratories, Inc., Aliso Viejo, CA, USA*
[3]*Department of Pathology and Laboratory Medicine, Brown University Warren Alpert Medical School, Lifespan Academic Medical Center, Legorreta Cancer Center at Brown University, Providence, RI, USA*
[4]*Tumor Microenvironment and Metastasis Program, Indiana University Melvin and Bren Simon Comprehensive Cancer Center, Indianapolis, IN, USA*

Correspondence

Liang Cheng, Department of Pathology and Laboratory Medicine, Brown University Warren Alpert Medical School, Lifespan Academic Medical Center; Legorreta Cancer Center at Brown University, Providence, RI 02912, USA.
Email: liang_cheng@brown.edu

Xin Lu, Tumor Microenvironment and Metastasis Program, Indiana University Melvin and Bren Simon Comprehensive Cancer Center, Indianapolis, IN 46202, USA.
Email: xlu@nd.edu

Xuechun Wang and Anna Juncker-Jensen are co-first authors with equal contributions

ORCID

Liang Cheng https://orcid.org/0009-0004-2260-6254
Xin Lu https://orcid.org/0000-0002-0284-6478

REFERENCES

1. Schumacher TN, Thommen DS. Tertiary lymphoid structures in cancer. Science. 2022;375(6576):eabf9419.
2. Coppola D, Nebozhyn M, Khalil F, Dai H, Yeatman T, Loboda A, et al. Unique ectopic lymph node-like structures present in human primary colorectal carcinoma are identified by immune gene array profiling. Am J Pathol. 2011;179(1):37–45.
3. Groeneveld CS, Fontugne J, Cabel L, Bernard-Pierrot I, Radvanyi F, Allory Y, et al. Tertiary lymphoid structures marker CXCL13 is associated with better survival for patients with advanced-stage bladder cancer treated with immunotherapy. Eur J Cancer. 2021;148:181–89.
4. Fridman WH, Meylan M, Petitprez F, Sun CM, Italiano A. Sautès-Fridman C. B cells and tertiary lymphoid structures as determinants of tumour immune contexture and clinical outcome. Nat Rev Clin Oncol. 2022;19(7):441–57.
5. Veglia F, Sanseviero E, Gabrilovich DI. Myeloid-derived suppressor cells in the era of increasing myeloid cell diversity. Nat Rev Immunol. 2021;21(8):485–98.
6. Zhang H, Ye YL, Li MX, Ye SB, Huang WR, Cai TT, et al. CXCL2/MIF-CXCR2 signaling promotes the recruitment of myeloid-derived suppressor cells and is correlated with prognosis in bladder cancer. Oncogene. 2017;36(15):2095–104.
7. Balar AV, Galsky MD, Rosenberg JE, Powles T, Petrylak DP, Bellmunt J, et al. Atezolizumab as first-line treatment in cisplatin-ineligible patients with locally advanced and metastatic urothelial carcinoma: a single-arm, multicentre, phase 2 trial. Lancet. 2017;389(10064):67–76.
8. Condamine T, Dominguez GA, Youn JI, Kossenkov AV, Mony S, Alicea-Torres K, et al. Lectin-type oxidized LDL receptor-1 distinguishes population of human polymorphonuclear myeloid-derived suppressor cells in cancer patients. Sci Immunol. 2016;1(2):aaf8943.

9. Wang G, Lu X, Dey P, Deng P, Wu CC, Jiang S, et al. Targeting YAP-Dependent MDSC Infiltration Impairs Tumor Progression. Cancer Discovery. 2016;6(1):80–95.

10. Ravi A, Hellmann MD, Arniella MB, Holton M, Freeman SS, Naranbhai V, et al. Genomic and transcriptomic analysis of checkpoint blockade response in advanced non-small cell lung cancer. Nat Genet. 2023;55(5):807–19.

SUPPORTING INFORMATION

Additional supporting information can be found online in the Supporting Information section at the end of this article.